Applied Catalysis B: Environmental 187 (2016) 310–327

Contents lists available at ScienceDirect

Applied Catalysis B: Environmental

journal homepage: www.elsevier.com/locate/apcatb

Catalytic steam gasification of pinewood and eucalyptus sawdust using reactive flash volatilization

Fan Liang Chan, Akshat Tanksale*

Department of Chemical Engineering, Monash University, Clayton, VIC 3800, Australia

ARTICLE INFO

Article history:
Received 8 October 2015
Received in revised form 15 January 2016
Accepted 17 January 2016
Available online 21 January 2016

Keywords:
Catalytic steam gasification
Reactive flash volatilisation
Pinewood
Eucalyptus
Nickel catalyst

ABSTRACT

Catalytic steam gasification of cellulose using reactive flash volatilisation (RFV) has been proven as a promising approach for syngas production. However, using cellulose as feedstock is economically unfavourable. This paper investigates the production of syngas using RFV of pinewood and eucalyptus sawdust as feedstock. Experiments were conducted to evaluate the effects of catalyst promoters, carbon to oxygen ratio, carbon to steam ratio, feedstock type and ash contents on product yields (i.e. gas, tar and char) and product gas composition. High gasification efficiency and low char selectivity were observed in the pinewood RFV with Re-Ni and Rh-Ni catalysts, which can be explained by the catalysts high active metal substrate dispersion. Additionally, in comparison to cellulose, higher gasification efficiencies were also observed in the pinewood and eucalyptus RFV. This can be attributed to the effects resulted from higher amorphous structure of lignocellulosic biomass compared to microcrystalline cellulose, and the catalytic effects of alkali and alkaline earth metals (AAEM species) found in the lignocellulosic biomass ash. The catalytic effects o f AAEM species further reduced the coke deposition on the Ni catalysts, making the effect of noble metal promoter on the Ni catalysts less significant. The effects on product yields and gas composition from promoters, carbon to oxygen ratio and carbon to steam ratio were less pronounced.

1. Introduction

With the growing concerns on climate change and greenhouse gas emissions, there is an urgent need for global transition from fossil based energy sources to renewable energy sources. Lignocellulosic biomass, as a renewable and carbon neutral energy source, is recognized as one of the most promising solutions for this issue due to its wide availability. Lignocellulosic biomass is the most abundant renewable biomass which has an estimated annual production of 10 billion MT [1].

There are a number of conversion technologies for utilizing biomass as renewable energy resource, such as thermal conversion (combustion), biochemical conversion (anaerobic digestion and fermentation), agrochemical conversion (oil extraction) and thermochemical conversion (pyrolysis, gasification, liquefaction, etc.) [2]. Among all the processing technologies, thermochemical biomass gasification receives the most interests from both industrial and academic researchers because of its high conversion efficiency and feedstock flexibility [3,4]. Synthesis gas can be produced *via* conventional biomass gasification in fluidised bed reactors at moderate temperatures, usually >700 °C. However, the product gas, in most cases, contains high concentration of undesired by-products such as tar and soot, which makes it unsuitable for use in downstream applications such as fuel cell [5]. Furthermore, accumulation of tar in the reactor may also lead to severe operational issues such as corrosion and clogging. Generally, downstream conversion of char and tar is necessary for the clean-up of synthesis gas.

Our previous publication demonstrated that clean synthesis gas can be produced *via* reactive flash volatilization (RFV) over nickel based catalysts using cellulose as the feedstock [6]. RFV is a complex process which involves pyrolysis, partial oxidation, steam reforming and water gas shift reactions. With carbon space velocity and carbon mass flow rate of 10–100 times higher than conventional fluidised bed reactors, tar free synthesis gas can be produced in a single fixed bed reactor allowing a short residence time of less than 50 ms. However, it is economically unfavourable to use microcrystalline cellulose as feedstock because biomass pre-treatment represents one of the most expensive steps in the processing of lignocellulosic biomass. In fact, the capital investment cost and operating cost of biomass pre-treatment process for a bioethanol production plant can be as high as 19% of the total capital expenditure and 32–38% of the total operating expenditure, respectively [7,8]. Therefore, it is more cost effective to use whole lignocellu-

* Corresponding author.
E-mail addresses: akshat.tanksale@monash.edu, akshattanksale@gmail.com (A. Tanksale).

http://dx.doi.org/10.1016/j.apcatb.2016.01.042
0926-3373/

losic biomass such as pinewood and eucalyptus wood waste with minimal pre-treatment.

In addition, it has been widely reported that catalytic effects from the inherent alkali and alkaline earth metals (AAEM species) in raw biomass can be beneficial to the gasification process as it accelerates the conversion of biochar and leads to higher gaseous product yield [9–13].

Therefore, in the present work, RFV of untreated pinewood and eucalyptus sawdust over promoted nickel based catalysts were investigated. The focus of this study was to evaluate the effects of carbon to oxygen (C/O), carbon to steam (C/S) ratio, biomass feedstock and inherent alkali and alkaline earth metals species (AAEM species) on product yields.

2. Experimental

2.1. Biomass

Softwood (pinus radiata, referred to as pinewood henceforth, 550 μm) and hardwood (eucalyptus regnans, referred to as eucalyptus henceforth, 500 μm), obtained from Pollard's Sawdust Supplies, Victoria, Australia, were used as feedstock in this investigation.

2.2. Biomass characterization

Physical and chemical properties of the biomass were characterized according to the European Standards (EN) or Australian Standards (AS). Moisture content of the biomass was determined according to EN14774. Ash yield was determined according to EN14775. Volatile matter, carbon, hydrogen and nitrogen content were determined according to EN15148:2009. Sulphur was determined according to AS1038.6.3.3.

Elemental analysis of the alkali and alkaline earth metals in biomass was performed using an Ametek Spectro iQ II X-Ray Florescence (XRF) Spectrometer. Biomass ashing was carried out by heating 25 g of the sample in air at 600 °C for 6 h. Ash residue was then recovered and subjected to XRF elemental analysis.

2.3. Catalyst

Three nickel based catalysts: Ru-Ni, Rh-Ni and Re-Ni supported on γ-alumina were developed using wet impregnation method. These bimetallic catalysts had nickel content of 10 wt% and noble metal promoter content of 1 wt%. Detailed synthesis procedures and characterizations of these catalysts can be found in our previous publication [6].

2.4. Reactor setup

Catalytic activity evaluation was conducted in a bench-scale reactor setup. Detailed description of the setup can be found in our previous publication [6].

Approximately 1 g of the promoted nickel catalyst was loaded onto fritted disc mounted at the centre of a 25 mm OD, 700 mm long quartz reactor before housed in an electric furnace. Prior to

Table 1
Physical and Chemical properties of Pinewood and Eucalyptus Sawdust.

	Pinewood Sawdust	Eucalyptus Sawdust
Properties		
Acidity (pH)	3.5–4.6	Not Available
Colour	cream to light brown	light to dark brown
Density	12–18 pounds/cubic feet	Not Available
Solubility in water	<0.1%	highly insoluble
Specific Gravity	0.5–0.8	Not Available
Particle Size	<550 micron	<500 micron
Proximate analysis (% db)		
Moisture Content,% ar (EN14774)	7.70	9.80
Ash Yield (EN14775)	0.80	7.30
Volatile	84.1	76.6
Fixed Carbon	15.1	16.0
Ultimate analysis (% db)		
Carbon	50.1	47.3
Hydrogen	6.20	5.30
Nitrogen	0.12	0.14
Sulphur	0.03	0.04
Oxygen[a]	42.8	39.9
Ash analysis (%)		
MgO	30.95	33.08
Al_2O_3	2.59	6.73
SiO_2	3.40	26.1
P_2O_5	11.27	3.20
SO_3	6.51	5.11
Cl	3.30	6.95
K_2O	22.35	4.14
CaO	17.55	11.33
TiO_2	0.12	0.46
V_2O_5	Not Available	0.05
Cr_2O_3	0.04	0.12
MnO	1.19	0.48
Fe_2O_3	0.38	1.97
CoO	0.09	0.10
NiO	0.06	0.01
CuO	0.01	0.02
ZnO	0.09	0.05
Ga	0.01	Not Available

[a] Calculated by difference.

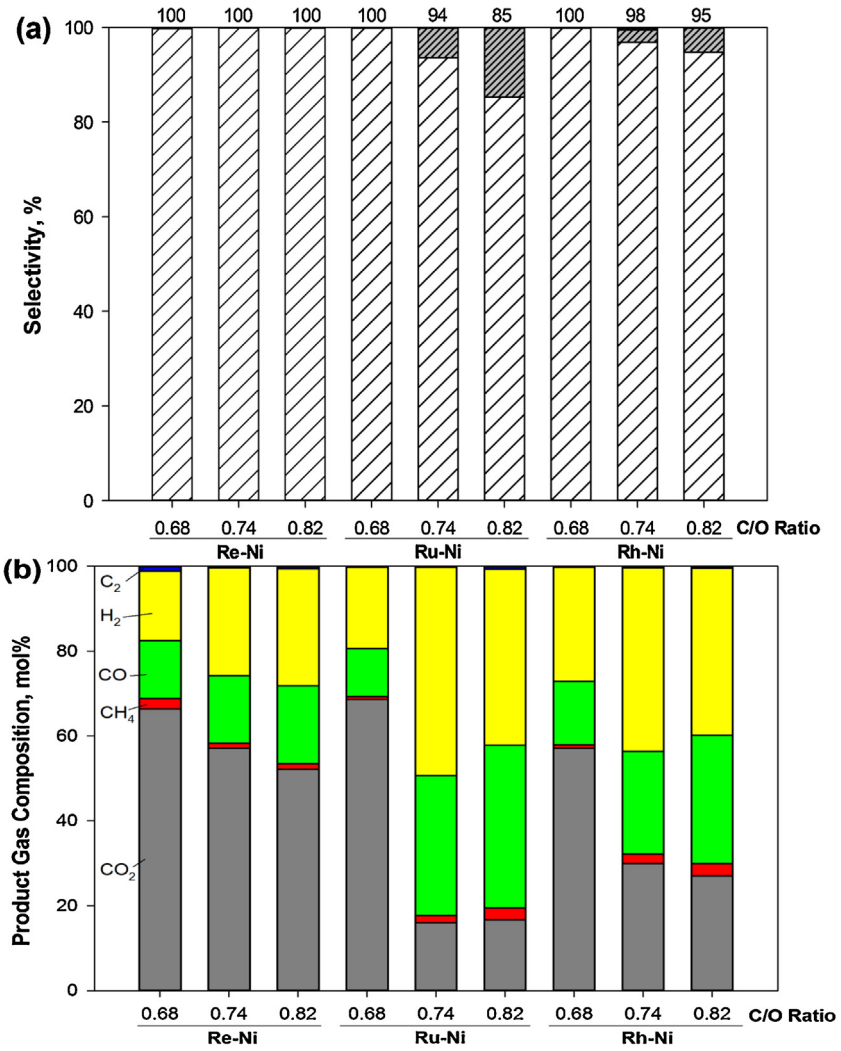

Fig. 1. Effect of C/O feed and catalyst promoters on: (a) selectivity of gas (white), char (grey) and tar (black) based on carbon balance. The numbers on the top of each bar represent gasification efficiency, which is the percentage of carbon in gas and tar combined; and (b) product gas composition. C_2 compounds include ethane, ethylene and acetylene. Reaction conditions: Pinewood sawdust flow rate = 15 g h^{-1}, 750 °C, C/S = 1.17. Here tar is defined as water-soluble organics.

each experiment, the catalyst was reduced in H_2/N_2 gas mixture at 400 °C for 4 h. The RFV experiment was carried out at the temperature of 750 °C, which was found to be optimum from our previous studies [6,14]. During the experiment, 15 g/h of pinewood or eucalyptus sawdust was screw-fed from a K-Tron powder feeder in co-current gas flow into an isothermal reactor. The amounts of steam and oxygen fed into the reactor were determined based on the C/O and C/S ratios of the experiment. C/O ratio is defined as the ratio of carbon atoms in the feedstock to the oxygen atoms in the O_2 feed gas. Nitrogen was used as make-up gas for maintaining the reactor space velocity. Exiting gas from the reactor was fed into a custom built gas–liquid separator where the gas samples were periodically analysed using a Shimadzu gas chromatograph GC-2014 and liquid product was collected in the separator. Volumetric flow rate of the product gas was also determined using a 50 ml soap bubble flow meter.

Moles of carbon atoms in the gas phase were calculated by measuring the amount of carbonaceous molecules in the gas phase using the gas chromatographer. Moles of carbon atoms in the liquid phase (tar) were calculated by measuring the total organic carbon in the condensate using Shimadzu TOC-L series analyser. Liquid sample was diluted with deionised water to a ratio of 1:400 before the analysis. Moles of carbon atoms in the solid product (biochar) were calculated based on the amount of carbon dioxide and carbon monoxide produced in the temperature programmed oxidation of biochar in the homemade setup used for the temperature programmed reduction and CO-desorption, as illustrated in our previous publication [6]. By summing up the cumulative moles of carbon atoms in gas, liquid and solid products collected throughout the experiment, overall carbon balance of the run can be calculated. Based on the carbon balance, selectivity for gas, tar and char are computed according to the following equations —

$$S_{gas} = \frac{\text{Moles of Carbon atoms in the gas phase}}{\text{Moles of Carbon atoms in the products}} \times 100\%$$

$$S_{Tar} = \frac{\text{Moles of Carbon atoms in the liquid phase}}{\text{Moles of Carbon atoms in the products}} \times 100\%$$

$$S_{char} = \frac{\text{Moles of Carbon atoms in the solid phase}}{\text{Moles of Carbon atoms in the products}} \times 100\%$$

The carbon atom balance between the set feed rate and the measured products rate was found be within ± 5.32% which is acceptable due to experimental errors.

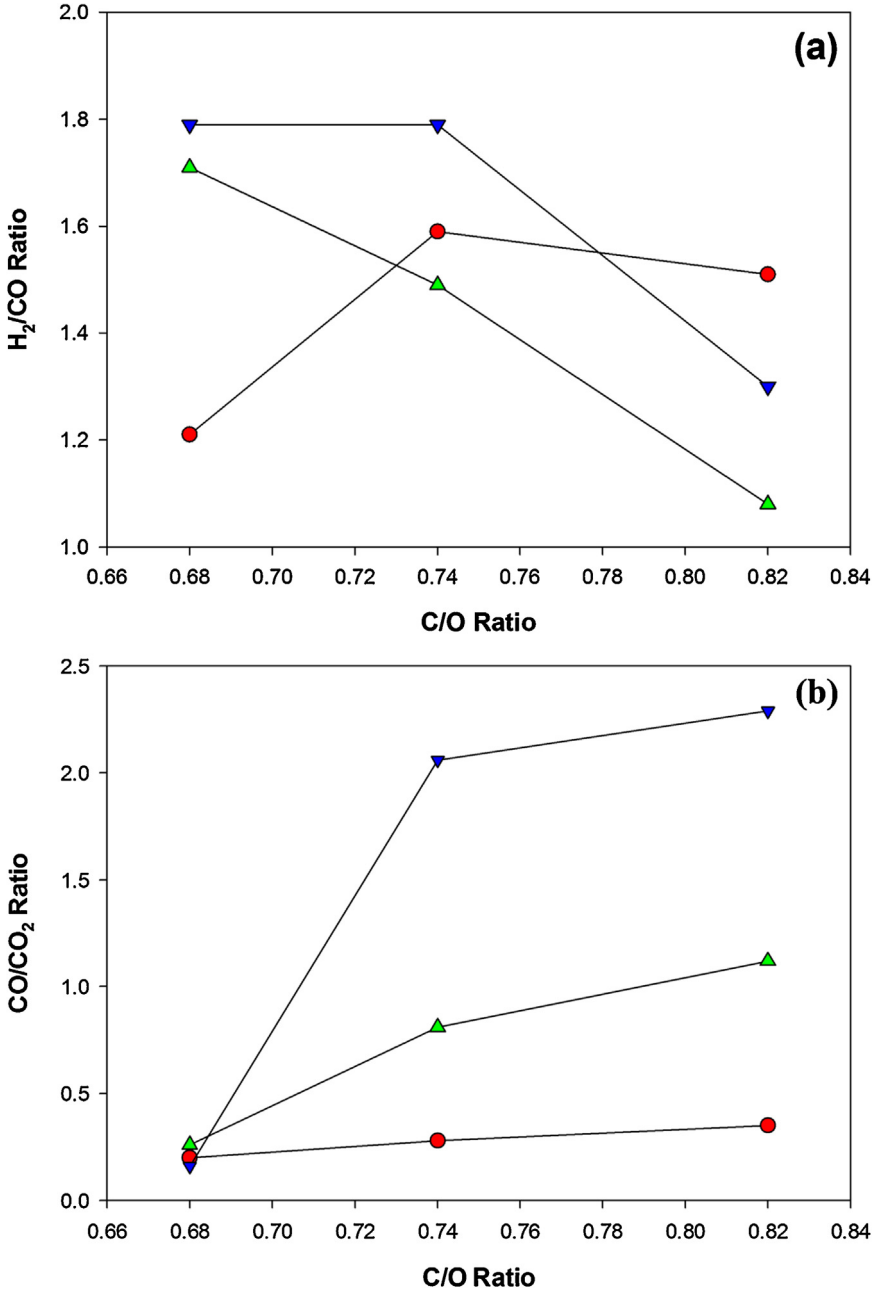

Fig. 2. Effect of carbon to oxygen ratio on (a) H_2:CO ratio and (b) CO:CO_2 ratio of promoted nickel based catalysts on γ-alumina support at pinewood sawdust flow rate = 15 g h^{-1}, temperature of 750 °C and C/S ratio of 1.17. (●) Re-Ni, (▼) Ru-Ni (▲) Rh-Ni.

2.5. Catalyst characterisation

Powder X-ray diffraction measurements of fresh and spent nickel catalysts were carried out in a Rigaku Miniflex powder diffractometer with mono-chromatized Cu Kα radiation (λ = 0.154 nm) at 40 kV and 15 mA.

TEM specimens were prepared using a solvent method. A small amount of catalyst powder and a few millilitre of solvent (butanol) were placed in an agate mortar. The catalyst power was then gently ground in the solvent until a sufficient amount of fine material was suspended in the solution. A holey carbon coated copper grid (the TEM sample grid) was then dipped in the solution and the prepared TEM specimen was left to dry at room temperature.

Size and morphology of the fresh and spent catalyst nanoparticles were studied using FEI Tecnai G2 F20 S-TWIN Field Emission Gun (FEG) Scanning Transmission Electron Microscope (TEM). Energy Dispersive X-Ray Spectroscopy (EDS) mapping of nickel, noble metal and various alkali and alkaline earth metals species on spent catalysts were carried out in the STEM mode using a high angle annular dark field (HAADF) Windowless X-ray detector (Bruker Quantax 400). The STEM was operated at 200 kV at magnifications of between 40,000 ~ 225,000 times with 20° of specimen tilt. Collected EDS maps have a resolution of 512 × 512 pixels.

3. Results and discussion

3.1. Biomass characterisation

Physical and chemical properties of pinewood and eucalyptus sawdust used in this study are presented in Table 1. Results from

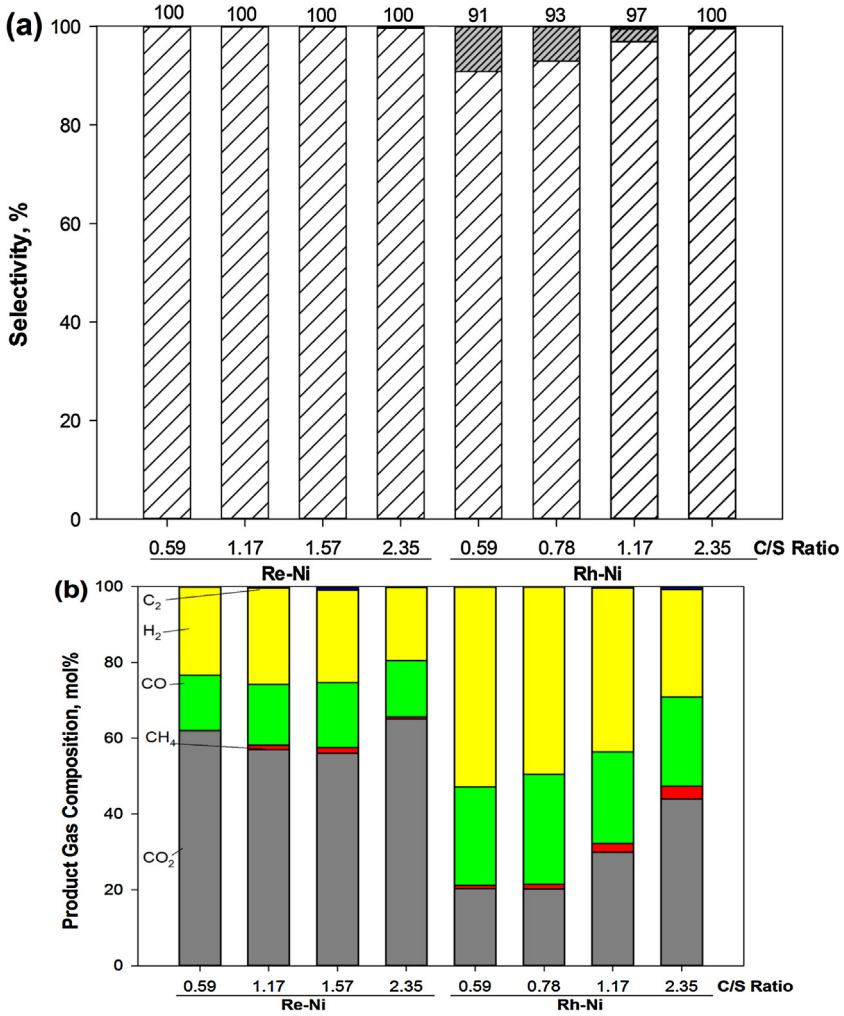

Fig. 3. Effect of C/S feed ratio and catalyst promoters on: (a) selectivity of gas (white), char (grey) and tar (black) based on carbon balance. The numbers on the top of each bar represent gasification efficiency, which is the percentage of carbon in gas and tar combined; and (b) product gas composition. C_2 compounds include ethane, ethylene and acetylene. Reaction conditions: Pinewood sawdust flow rate = 15 g h^{-1}, 750 °C, C/O = 0.74. Here tar is defined as water-soluble organics.

the proximate analysis showed that eucalyptus sawdust had ~9 times higher ash content, lower volatile matter and roughly similar fixed carbon content, in comparison to pinewood sawdust. Carbon, hydrogen and oxygen composition in the two samples were similar, as reported in the ultimate analysis. XRF analysis of the ashes revealed the composition differences of alkali and alkaline earth metals (AAEM species) in the biomass ash. Common compounds found in these two biomass ashes include oxides of magnesium, calcium, potassium, silica, phosphorous, sulphur and chlorine. Both samples contained roughly similar composition of magnesium oxide. However, pinewood ash contained higher level of phosphorous and potassium oxides whereas eucalyptus ash had more silica.

3.2. Effect of carbon-to-oxygen ratio in RFV of pinewood sawdust

The effect of carbon to oxygen feed ratio (C/O) was tested on all three promoted catalysts. Based on our previous studies [6], the optimum feed rate of pinewood sawdust was kept constant at 15 g/h, while the oxygen was fed at the rate of 143 (C/O = 0.82), 158 (C/O = 0.74) and 173 SCCM (C/O = 0.68). Reactor temperature and C/S ratio for these runs were kept constant at 750 °C and 1.17, respectively.

Test results are illustrated in Fig. 1. Products selectivity (i.e. gas, char and tar) are calculated based on the carbon atom balance. The product gas composition is measured on a dry basis, whereas water yield is not reported. As seen in Fig. 1(a), Re-Ni catalyst exhibited high gas yield (>99%) in all three C/O ratios. Combined tar and char yields were less than 1%. However, with Rh-Ni and Ru-Ni catalysts, decrease in gas yield and increase in char yield were observed with the increase of C/O ratio. This result is consistent with the findings from our previous study on reactive flash volatilisation of cellulose [6]. Higher oxygen feed (low C/O) leads to higher catalyst bed temperature, which favours steam reforming and oxidation reactions, and therefore the higher gas yield. Although gas yields were higher, the quality of the syngas produced was lower. This is because higher oxygen input also causes further oxidation of CO into CO_2 and H_2 into H_2O, leading to decrease in product gas heating value. This can be seen with all the three catalysts where CO_2 mole percent were the highest at C/O of 0.68 and decreased as the C/O ratio increased.

Although the non-volatile fraction of the pinewood sawdust is higher than the microcrystalline cellulose studied in previous publication, char yields were substantially lower in RFV of pinewood sawdust in comparison to RFV of microcrystalline cellulose under similar reaction conditions. This can be explained by three reasons –

a Higher amount of amorphous structure (hemicellulose and lignin) and lower crystalline structure in pinewood sawdust resulted in faster devolatilisation, therefore, lower char pro-

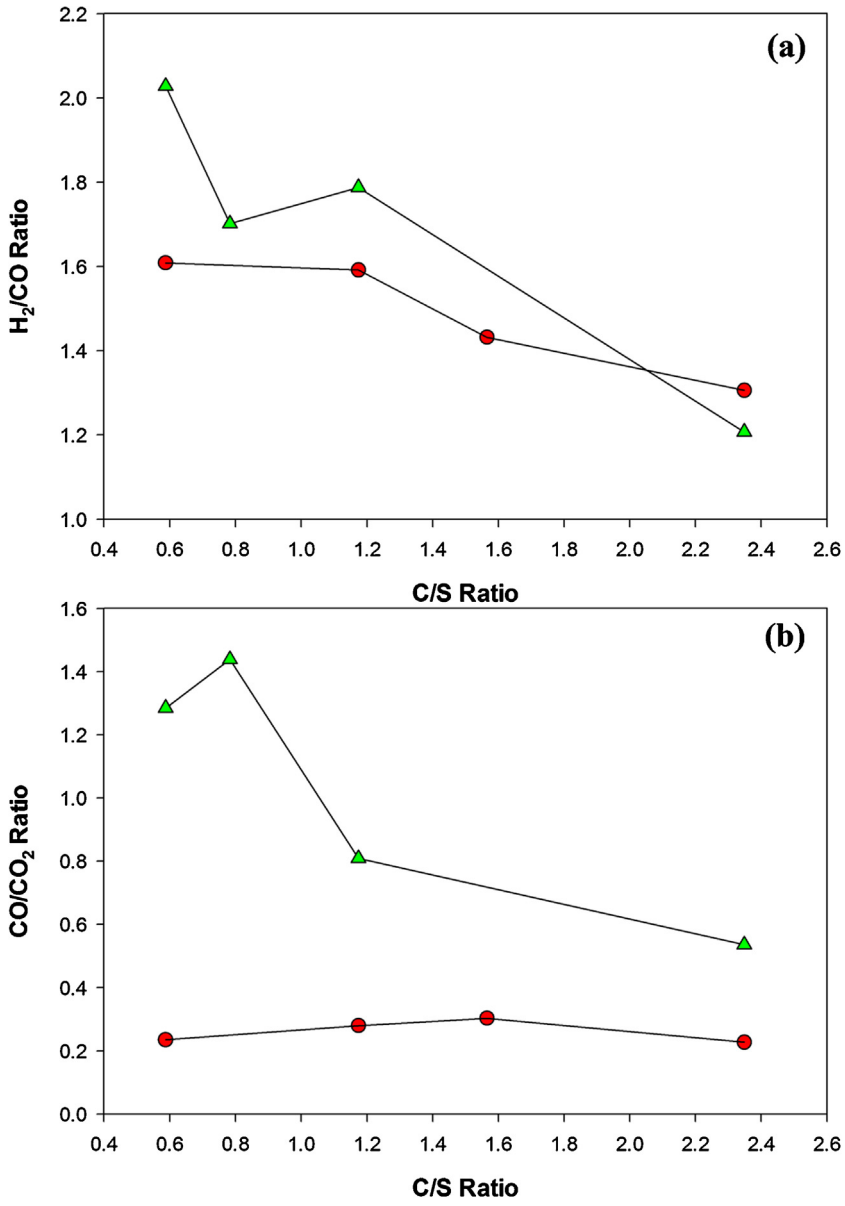

Fig. 4. Effect of carbon to steam ratio on a) H_2:CO ratio and b) CO:CO_2 ratio of promoted nickel based catalysts on γ-alumina support at pinewood sawdust flow rate = 15 g h^{-1}, temperature of 750 °C and C/O ratio of 0.74. (●) Re-Ni and (▲) Rh-Ni.

duction. Amorphous hemicellulose and lignin are known to have faster devolatilisation due to their lower pyrolysis onset temperatures and the reactions exothermic properties [14]. Since 48.6–63% by mass of pinewood is hemicellulose and lignin [15–17], faster devolatilisation can be expected. Also, lower cellulose content per unit feed reduces the production of secondary and tertiary tar which are precursors for char production. Levoglucosan, an anhydrosugar derivative from pyrolytic decomposition of cellulose, is known to undergo secondary decomposition reactions to form secondary tar [14,18–20]. Because only 37.0–51.4% by mass of pinewood sawdust is cellulose, amount of levoglucosan produced from cellulose pyrolysis is substantially lower than in RFV of cellulose, and therefore, reduces the amount of char produced from this secondary reaction.

b Synergistic effect between lignocellulosic components (i.e. cellulose, hemicelluloses and lignin) enhances the production of low molecular weight products and leads to lower char production [21,22]. The synergy is particularly effective between pyrolytic decomposition products of cellulose and lignin. Lignin-derived products inhibit thermal polymerization of levoglucosan and the formation of 1,6-anhydro-b-D-glucofuranose while other cellulose derived products inhibit low molecular weight products from carbonisation in vapour phase. In the co-pyrolysis of cellulose and lignin, the presence of lignin derived phenolic products, such as guaiacol (2-methoxyphenol; *o*-methoxyphenol), 4-methylguaiacol (Creosol; 2-methoxy-4-methylphenol) and 4-vinylguaiacol (4-ethenyl-2 methoxyphenol), help to enhance the production of levoglucosan, glycolaldehyde, hydroxyacetone and other low molecular weight products by altering the formation mechanisms of these androsugars and secondary degradation mechanisms of the volatile species [22]. Therefore, char production was lower. Similar findings have been reported elsewhere [21,23]. The effectiveness of these phenolic derivatives in inhibiting char formation can be explained with the hydrogen-acceptor/donor theory [23]. It appears that these phenolic derivatives may act as a strong hydrogen donor by providing hydrogen radical to unstable radical compounds formed during

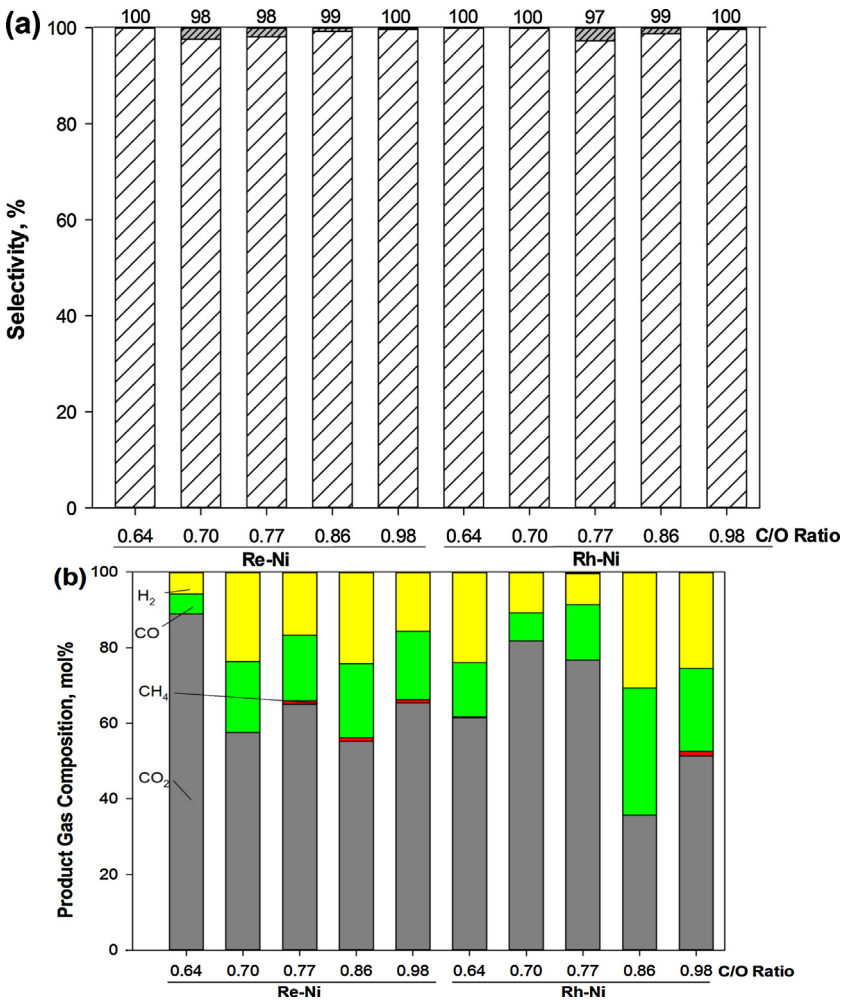

Fig. 5. Effect of C/O ratio in RFV of eucalyptus sawdust on: (a) selectivity of gas (white), char (grey) and tar (black) based on carbon balance. The numbers on the top of each bar represent gasification efficiency, which is the percentage of carbon in gas and tar combined; and (b) product gas composition. C_2 compounds include ethane, ethylene and acetylene. Reaction conditions: Pinewood sawdust flow rate = 15 g h^{-1}, 750 °C, C/S = 1.11. Here tar is defined as water-soluble organics.

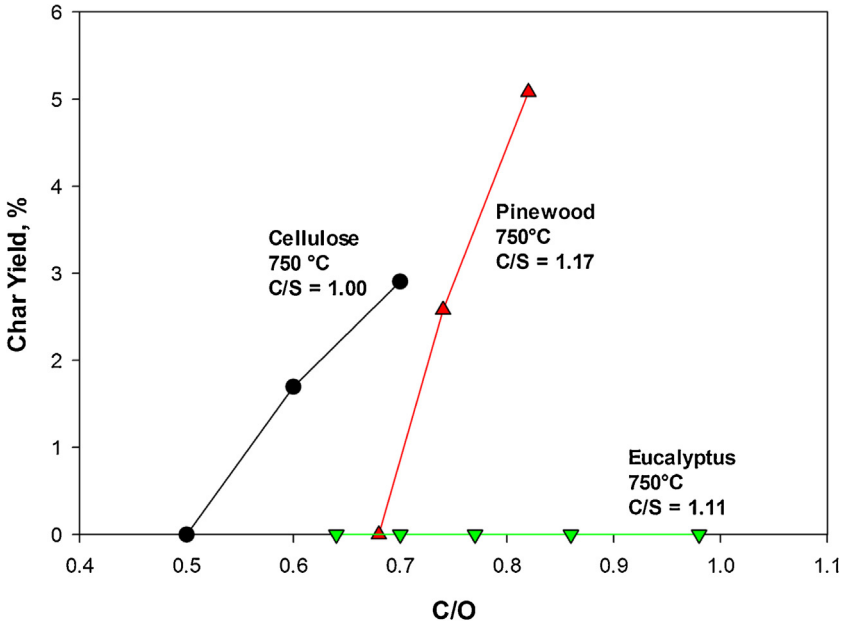

Fig. 6. Comparison of char yield of different biomass feedstock.

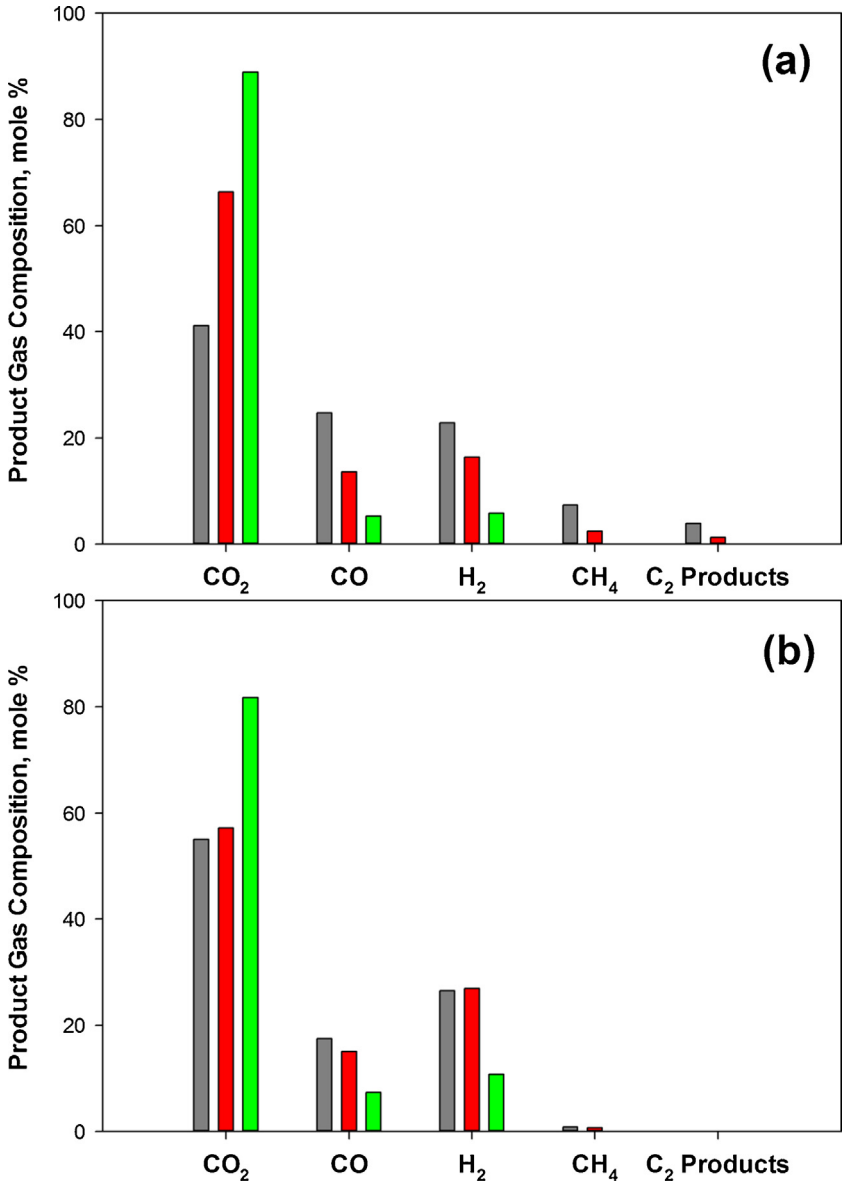

Fig. 7. Comparison of product gas composition of RFV with different biomass feedstocks at 750 °C. (a) Re-Ni (Cellulose, C/O-0.6, C/S-1.0, Pinewood, C/O-0.68, C/S-1.17 and Eucalyptus, C/O-0.64, C/S-1.11) (b) Rh-Ni (Cellulose, C/O-0.7, C/S-1.0, Pinewood, C/O-0.68, C/S-1.17 and Eucalyptus, C/O-0.7, C/S-1.11).

the pyrolysis process which otherwise would undergo radical coupling reactions that leads to char formation.

c Inherent alkali and alkaline earth metals (AAEM species) retained in the char catalyse gasification reaction, resulting in faster char decomposition, therefore, lower char yield. It is known in literature that AAEM species, particularly potassium (K), are effective catalysts in promoting C—C bond cleavage reactions and char gasification [24–26]. The mechanism of how these AAEM species catalyses char gasification remains unclear, but some studies have attributed this enhanced catalytic activity to an oxygen transfer cycle occurring during the gasification, with either carbon reduction or oxygenated complexes decomposition promoted under the presence of AAEM species [13].

With Re-Ni catalyst, a linear correlation can be observed between the increase in C/O ratio and the increase in the production of oxygen deficient compounds- H_2 and CO (Fig. 1(b)). With Rh-Ni and Ru-Ni catalysts, however, H_2 and CO compositions increased with the increase in C/O ratio, the actual production rate per unit gram of pinewood feed were, in fact, lower at higher C/O ratio. The higher H_2 and CO gas percentages in gas stream resulted from significant reduction in the product gas flow rate (not reported), caused by deposition of char in the reactor, which led to clogging and therefore, reduced the output gas flow. Clogging can be avoided by using the conditions reported in the manuscript which do not produce char.

Re-Ni catalyst had the highest gasifying efficiency in RFV of pinewood sawdust. This can be attributed to the higher dispersion of the active metal substrate on the catalyst and higher activity in promoting oxidation [6]. Re can exist in multiple oxidation states, which is effective in promoting oxidation owing to its high oxidation state and cationic charge [27]. Re oxo-complexes, particularly methyl-rhenium trioxide (MTO), is widely used in oxidation of hydrocarbons because of this property. High CO_2 composition was also observed in RFV of pinewood sawdust over Re-Ni catalyst (Fig. 1(b)), which confirms that oxidation was the dominating reaction. As oxidation is a much faster and exothermic reaction, higher gasification efficiency can be expected with this catalyst [28,29].

In Fig. 2(a), a marginal increase in H_2:CO ratio of the product gas can be observed with increase in C/O ratio over Re-Ni catalyst.

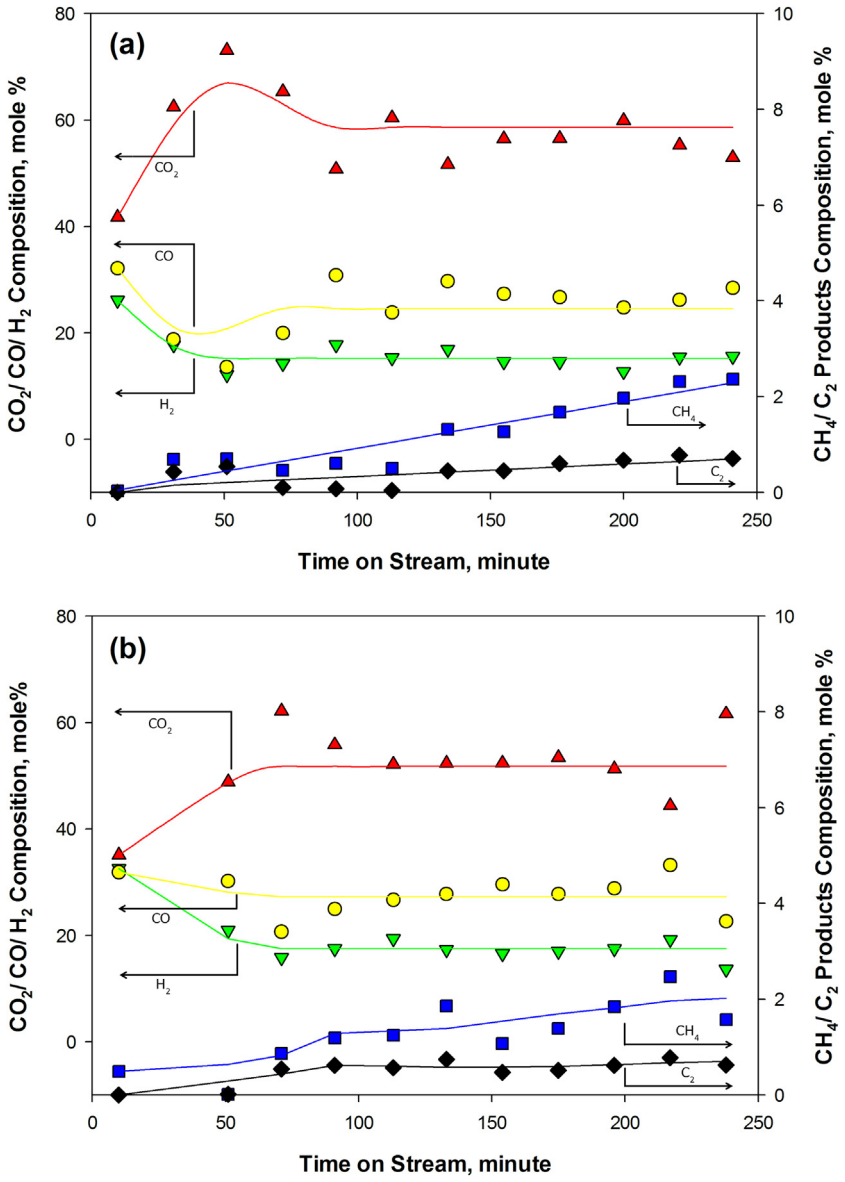

Fig. 8. Gas production evolutions over time-on-stream for pinewood sawdust flow rate = 15 g h^{-1}, and temperature of 750 °C using Re-Ni catalyst at (a) C/O = 0.74 (b) C/O = 0.82.

Higher H_2:CO ratios can be explained by a shift in the dominant reactions from oxidation to steam reforming and water gas shift reactions under low oxygen feed conditions. When using Ru-Ni and Rh-Ni as catalysts, the ratio of H_2:CO in the product gas decreased with the increase in C/O ratio. This implies that under high C/O ratio reaction conditions, Ru-Ni and Rh-Ni catalyst are less effective in promoting steam reforming and water gas shift reactions. Increase in C_2 products and char yields also suggest that the reactions over Ru-Ni and Rh-Ni suffered with slower thermal decomposition reaction.

In Fig. 2(b) a slight increase in CO:CO_2 ratio was observed with increase in C/O ratio in all Re-Ni runs, which is insignificant. With Rh-Ni and Ru-Ni as catalysts, increase C/O feed ratio led to increase in CO:CO_2 ratio, due to incomplete gasification.

Overall, the gasification efficiency of promoted nickel catalyst in RFV of pinewood sawdust was in the following order: Re-Ni > Rh-Ni > Ru-Ni. Only the Re-Ni catalyst was able to attain sustained operation at all three C/O ratios with negligible amount of char formed for a long period of time (>240 min).

3.3. Effect of carbon-to-steam ratio in pinewood sawdust RFV

The effect of carbon to steam feed ratio (C/S) was tested on two promoted catalysts- Re-Ni and Rh-Ni. Ru-Ni catalyst was not considered for this study due to high char selectivity observed in Section 3.2. In this study pinewood sawdust feed rate, reactor temperature and C/O ratio were kept constant at 15 g/h, 750 °C and 0.74, respectively, whereas C/S ratio was varied between 0.59 and 2.35.

Results obtained from the various C/S ratio runs are plotted in Fig. 3. Re-Ni catalyst was able to achieve gas yield of >99% in all C/S ratios (Fig. 3(a)). There was no char formed in any of runs, with <1% of carbonaceous products in tar. The high gas conversion and low char formation can be attributed to the use of Re as promoter, which favours exothermic oxidation under these reaction conditions. Nonetheless, it is expected that the fraction of tar increases with increasing C/S ratio (lower steam) as the steam reforming activity is lower.

The gasification efficiency of Rh-Ni catalyst was lower in all C/S ratios. Product gas yield increased with C/S ratio and was the highest at C/S ratio of 2.35. However, three out of the four runs

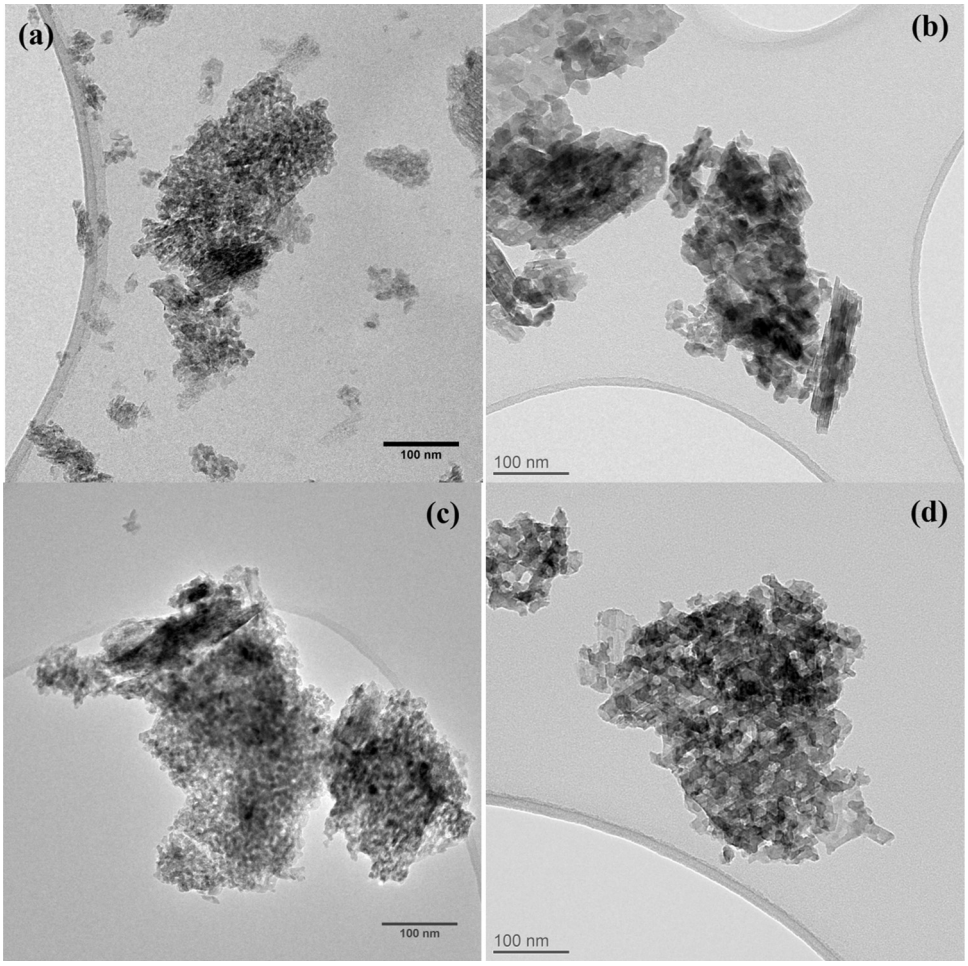

Fig. 9. TEM images of (a) Fresh Re-Ni catalyst. (b) Spent Re-Ni Catalyst from Pinewood RFV (750 °C, C/O— 0.68, C/S-1.17, Runtime- 255 min) (c) Fresh Rh-Ni (d) Spent Rh-Ni from Pinewood RFV (750 °C, C/O— 0.68, C/S-1.17, Runtime- 260 min). Scale bar = 100 nm.

resulted in sufficient char formation that caused partial clogging of the reactor. The lower catalytic activity can be attributed to the Rh promoter used, which is known to be more effective in promoting partial oxidation than complete oxidation [30,31]. Because the energy produced from partial oxidation is at least an order of magnitude lower than complete oxidation, to gasify the same amount of pinewood, higher energy input (and hence higher temperature) would be needed in Rh-Ni catalysed RFV in comparison to Re-Ni. This demand for higher energy input was further compounded by the high amount of steam fed, which led to reduction in temperature due to the endothermic steam reforming reaction, therefore, resulted in incomplete gasification (i.e. char formation). The gasification efficiency increased with lower C/S ratio (i.e. higher steam feed rate) which suggests that lower steam reforming activity is beneficial in case of Rh-Ni catalyst.

Although >99% of gas yield was achieved with Re-Ni catalyst, the quality of the product gas was poor. The product gas was rich in CO_2 (56–65%), followed by H_2 and CO (19–25% and 14–17%, respectively). The high CO_2 yield was resulted from the relatively low C/O ratio used in these experiments and the effectiveness of Re-Ni catalyst in promoting oxidation. Moreover, side reactions such as decarbonylation and decarboxylation which occur under high steam fraction environment may also contribute to the production of CO_2 and CO [32].

Fig. 4(a) shows H_2/CO decreases with increase in C/S ratio because of the reduction in water gas shift reaction activity under steam lean atmosphere. The decrease in H_2 yield can be seen with both catalysts as C/S ratio increased.

The effects of C/S ratio on CO/CO_2 ratio in the product gas were dependent on type of promoter. The CO/CO_2 ratio in the product gas of all Re-Ni runs were unaffected by the change in C/S ratio (Fig. 4(b)). However, with Rh-Ni catalyst, a clear reduction in CO/CO_2 ratio is observed at high C/S ratio. This difference is believe to be because Re-Ni catalyst is more in promoting complete oxidation compared to Rh-Ni. Under the oxygen rich environment (C/O = 0.74), oxidation reaction dominated the complex reaction scheme over the Re-Ni catalyst. Whereas partial oxidation and steam reforming reaction were favoured over Rh-Ni catalyst, which led to the strong correlation between C/S feed ratio and CO/CO_2 product ratio.

In summary, Rh-Ni catalyst was found to be more affected by the C/S feed ratio compared to Re-Ni runs. Since Re can exhibit multiple oxidation states, working in oxygen rich condition had little impact from the variation in C/S ratio. Overall, these results have showed that change in C/S ratio only has minimal effect in improving the final product gas composition under oxygen rich conditions.

3.4. *Effect of feedstock and alkali and alkaline earth metals in biomass RFV*

To study the effect of feedstock, and alkali and alkaline earth metals (AAEM species) in RFV, a comparison between pinewood and eucalyptus sawdust gasification is presented, since these two

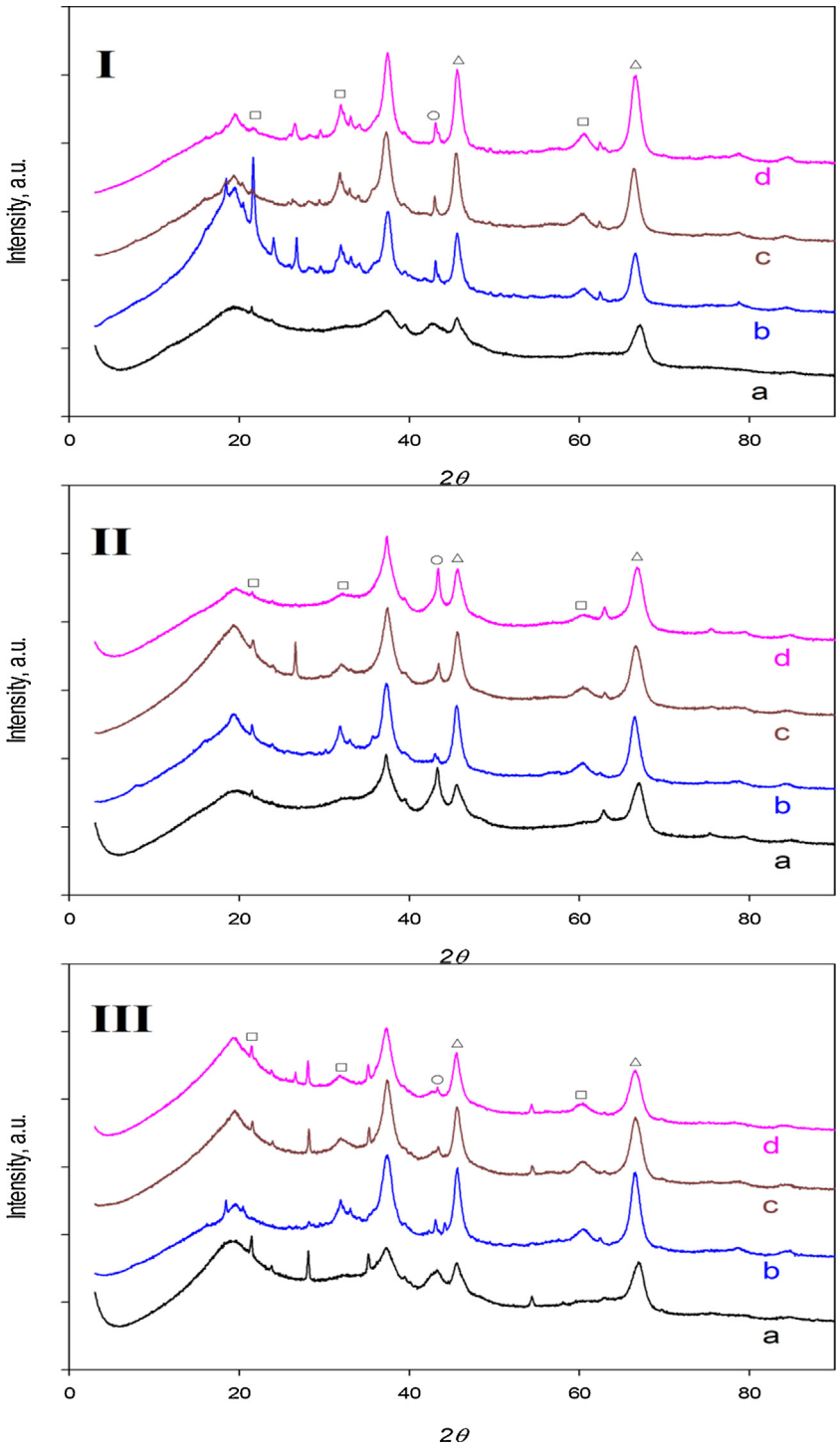

Fig. 10. Powder XRD patterns of Fresh and Spent Catalysts of Pinewood RFV- I) Re-Ni, II) Rh-Ni, III) Ru-Ni at different C/O ratios- a) Fresh Catalyst b) C/O-0.68 c) C/O-0.74 d) C/O-0.82. (△) γ-alumina (□) δ-alumina (○) NiO.

feedstocks had very different ash proportion and composition. As seen in Table 1, ash content of the eucalyptus sawdust used in this study was ~9 times higher than the pinewood sawdust. In this experiment, the eucalyptus sawdust feed rate was kept the same as in Section 3.2 and 3.3 at 15 g/h, while the oxygen feed was varied from 113 (C/O = 0.98) to 173 SCCM (C/O = 0.64), respectively. Reactor temperature and C/S ratio for these runs were kept constant at 750 °C and 1.11, respectively. Because of its high char selectivity reported in Section 3.3, Rh-Ni catalyst was of particular interest in this study.

The results (Fig. 5(a)) showed that all the runs with Rh-Ni and Re-Ni catalysts had >97% gas yield using eucalyptus sawdust as feedstock with no char formation. A comparison of char yield from RFV of cellulose, pinewood sawdust and eucalyptus sawdust under similar reaction conditions and Rh-Ni as catalyst is shown in Fig. 6. The effect of biomass ash content on enhancing char gasification can be clearly seen. RFV of cellulose (no ash) and pinewood sawdust (~1% ash) resulted in significant char formation at high C/O ratios of >0.6. However, no char formation was found in RFV of eucalyptus sawdust (~10% ash) even at C/O of 0.98. This confirms that

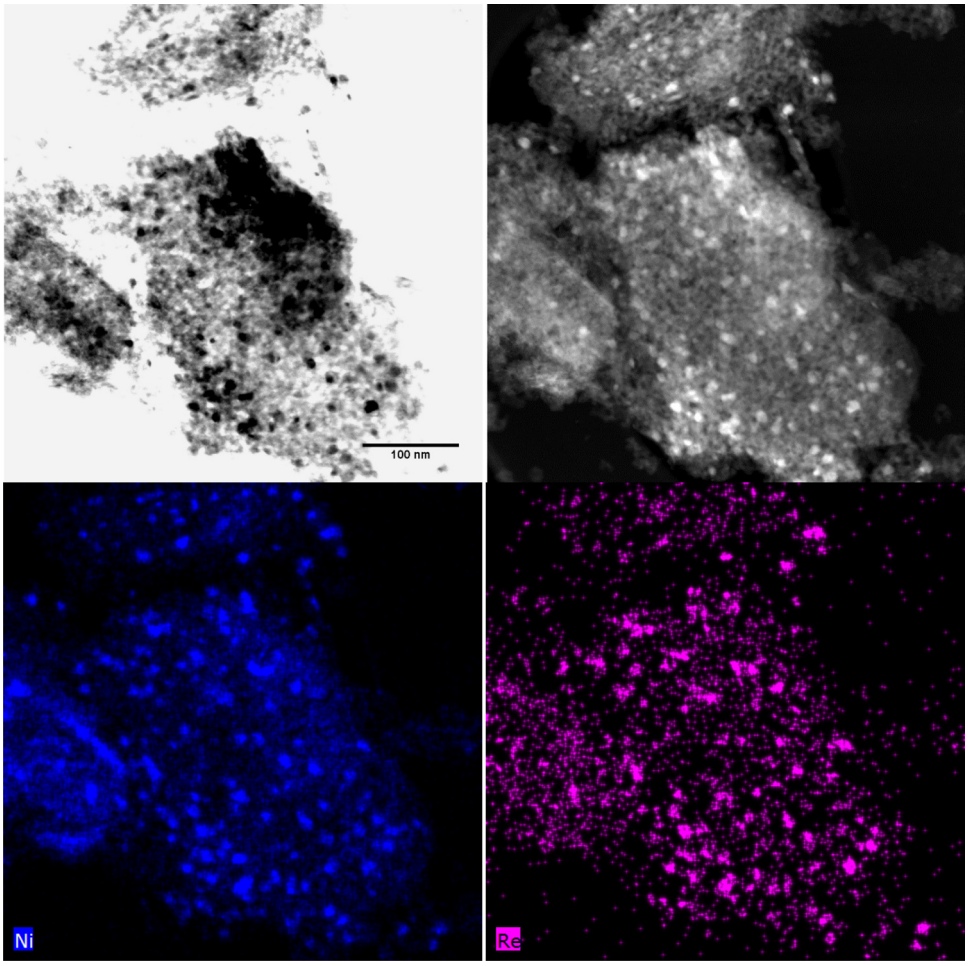

Fig. 11. TEM images of freshly reduced Re promoted nickel catalyst (a) bright field (b) high angle annular dark field and EDS elemental mapping of (c) Ni and (d) Re.

AAEM species in biomass play a critical role in enhancing char gasification as mentioned in Section 3.2. As for Re-Ni catalyst, results were consistent with previous finding that >98% of gas yield were attained.

The difference in gas and char yields observed in eucalyptus RFV can be explained by several reasons. Firstly, the variation in composition of cellulose, hemicellulose, lignin and ash in eucalyptus and pinewood sawdust lead to different thermal degradation behaviour in RFV. Secondly, differences in AAEM species composition of biomass result in different catalytic effects in RFV, which leads to different product distribution. Lastly, higher concentration of AAEM species retained in char further increases the rate of char gasification.

3.4.1. Biomass composition

Typically, eucalyptus contains 15–17 wt% hemicellulose, 38–49 wt% cellulose and 28–31 wt% lignin [15,33,34] in comparison to pinewood which contains 16–23 wt% hemicellulose, 37–51 wt% cellulose and 23–31 wt% lignin [15–17]. Higher hemicellulose and lignin content increases the rate of pyrolytic decomposition as discussed in our previous publication [14]. Moreover, hemicellulose and lignin in softwood and hardwood contain different types of compounds. Softwood (pinewood) hemicellulose contains galactoglucomannans, mannose and galactose units while hardwood (eucalyptus) hemicellulose contains glucuronoxylan, xylan and acetyl groups [15,35–39]. This difference between softwood and hardwood hemicellulose compounds has contributed to their different decomposition behaviour in pyrolysis. Previous studies have also reported faster devolatilisation rate and lower char yield in hardwood hemicellulose pyrolysis [36]. It has been shown that hardwood lignin also devolatilise at lower temperature and using less energy in comparison to softwood lignin [23,40]. This is due to the presence of syringyl lignin in hardwood, which promotes cell wall degradation [41]. Softwood contains guaiacyl rich lignin which has a higher softening point and hence much harder to depolymerise in comparison to syringyl rich lignin due to its branched structure and higher degree of polymerization [42].

3.4.2. Effect of AAEM species on tar destruction

Thermal polymerisation of anhydro-monosaccharides (i.e. levoglucosan) into polymers followed by successive dehydration is identified as one of the mechanisms of char production [43,44]. AAEM species such as K, Mg and Cl found in the eucalyptus sawdust are known to be effective in promoting the decomposition of tar and levoglucosan into low molecular weight species, such as CO_2, CO and water [12,45]. This explains the low tar yield during the RFV of eucalyptus sawdust, higher yield of CO_2 and CO (Fig. 5) and low yield of char (Fig. 7).

3.4.3. Effect of AAEM species on char gasification

Eucalyptus sawdust ash was ~9 times higher than pinewood sawdust, and therefore, higher rate of char gasification can be expected from the former biochar due to the catalytic effect of AAEM species such as K and Ca which lowers the gasification onset temperature [9–11].

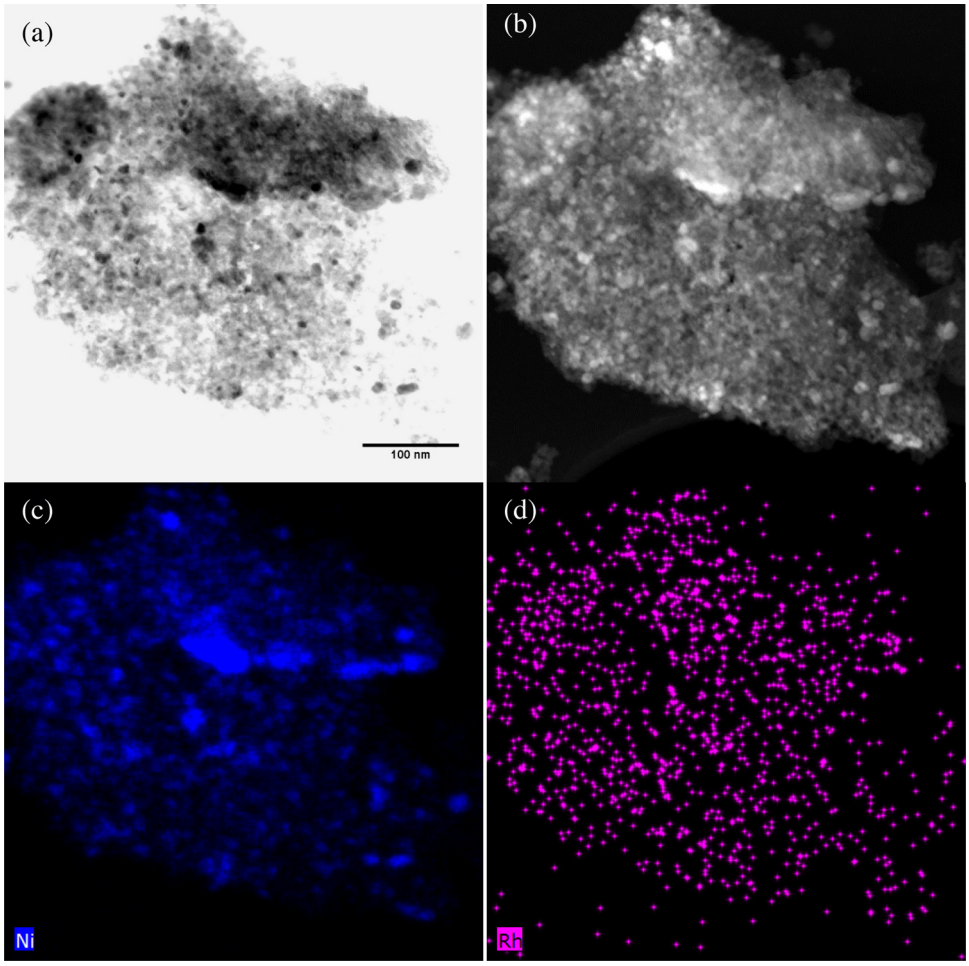

Fig. 12. TEM images of freshly reduced Rh promoted nickel catalyst (a) bright field (b) high angle annular dark field and EDS elemental mapping of (c) Ni and (d) Rh.

Although ash helps to lower the char yield, high ash content biomass makes a less desirable fuel due to the lower heating value of its gas product [46]. As shown in Fig. 5(b), large portion of the product gas generated in eucalyptus runs was CO_2. High calorific gas components such as H_2 and CO only accounted for 5.8–30.7% and 5.3–33.6% respectively. This may be explained by oxidation reaction triggered by AAEM species self-ignition at high temperatures under O_2 rich environment. Majority of the AAEM species in eucalyptus (Mg, Ca, K, P and S) have relatively low ignition temperatures. Therefore, under the operating condition of RFV, AAEM species and its derivatives can self-ignite and propagate combust in the product gas stream, leading to high CO_2 and water vapour production. In comparison to RFV of pinewood, RFV of eucalyptus resulted in increase in CO_2 yield by 51.8% and 92.7% using Re-Ni and Rh-Ni catalysts, respectively, under similar reaction conditions.

The effect of biomass ash content on product gas composition during RFV can be seen in Fig. 7. Using similar reaction conditions, CO_2 yield increased with ash content in biomass feedstock whereas other gas components such as H_2, CO, CH_4 and C_2 compound yields decreased. Higher condensate yield (i.e, water) was also observed, which suggests that the major reactions in RFV of eucalyptus sawdust were decarboxylation and oxidation, which are partly promoted by ash elements [12,47,48].

In comparison to the effect of AAEM species, the effect of noble metal catalysts on product distribution is insignificant. The catalytic effect of AAEM species is more dominant due to the high dispersion of AAEM species in the biomass feedstock. Because AAEM species is encapsulated within the biomass, gasification reactions are catalysed by these species immediately after pyrolytic decomposition. In contrast, partial oxidation and steam reforming of bio-oil (produced *in-situ*), catalysed by the porous catalyst particles used in the fixed bed, are slower, which may resulted from the diffusion limitation.

In summary, RFV of ash rich biomass feedstock such as eucalyptus sawdust was dominated by the catalytic effects from the AAEM species. However, these catalytic effects reduce the syngas quality by increasing CO_2 yield and lowering the calorific value.

3.5. Stability of catalyst

A comparison study of the catalyst stability used in RFV of pinewood and RFV of cellulose is presented in this section. As pointed out in our previous publications, deactivation of catalyst may happen due to thermal or chemical treatments resulting in structural changes in the catalyst, such as catalyst support phase transformation, active metal agglomeration and/or oxidation, poisoning, and carbon fouling [6,12]. Product gas evolution of two pinewood RFV runs with Re-Ni as catalyst, shown in Fig. 8, suggested that the selectivity of the catalyst was shifting slowly towards methane and C_2 compounds instead of CO and H_2. Composition of methane and C_2 compounds gradually increased from 0% to 1% and 3%, respectively. Similar increase in methane and C_2 products were also observed with Ru-Ni and Rh-Ni catalysts. The increase in minor products production can be attributed to the catalyst deactivation caused by Ni metal sintering at temperatures above 700 °C and partial oxidation of Ni° into NiO [49,50].

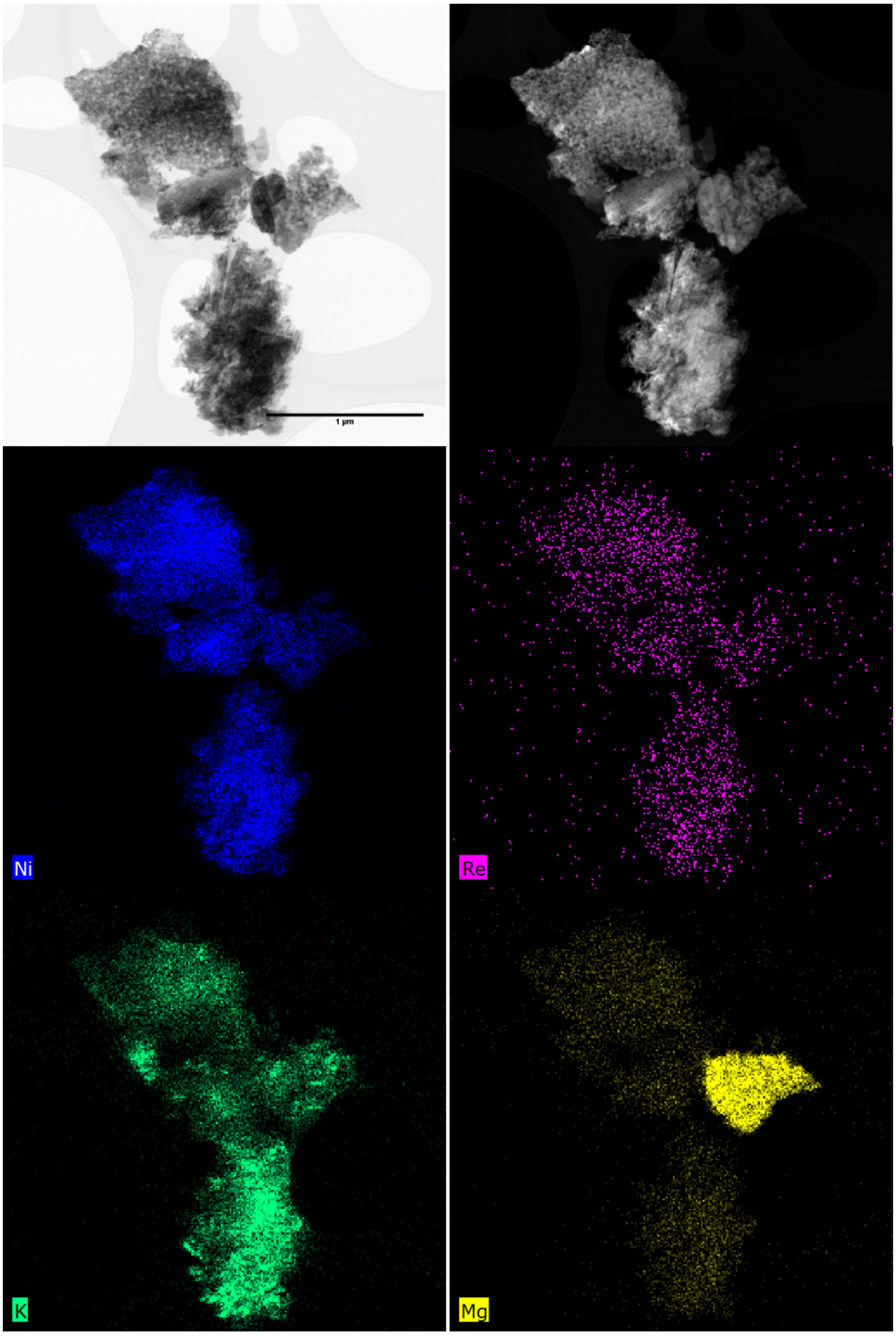

Fig. 13. Bright field, high angle annular dark field (HAADF) TEM images and TEM-EDS elemental distribution for Ni, noble metal promoter Re, K and Mg on spent Re-Ni catalyst from pinewood RFV. Reaction conditions: Pinewood flow rate = 15 g/h, Temperature = 750 °C, C/O = 0.68, C/S = 1.17 and Runtime = 255 min.

These minor products, particularly methane, are intermediate products produced directly from the decomposition of lignocellulosic biomass or hydrocarbons, which later are steam reformed into CO and H_2 on the catalyst [51,52]. However, when Ni metal is sintered/oxidized, this reduces the active metal surface on the catalyst, and therefore, reduces the catalytic activity and leads to higher production of these minor products. Methane may also be produced from the hydrogenation of CO (methanation reaction), however, given the presence of steam and the high temperature reaction conditions used, this reaction is highly unfavourable. Poisoning by feedstock ash (i.e. sulphur) is another cause which may contribute to the deactivation of catalyst [53,54].

Morphology of the fresh and spent Re-Ni and Rh-Ni catalysts was studied with a TEM and the results are shown in Fig. 9. Unlike our previous finding, the spent catalysts did not show significant change in their structure and no visible filamentous carbon deposition was found compared to the catalysts used in RFV of cellulose. However, some agglomeration may be seen in alumina particles of the spent catalyst. Partial phase transformation of γ–alumina into δ–alumina was confirmed in the XRD results (Fig. 10), which

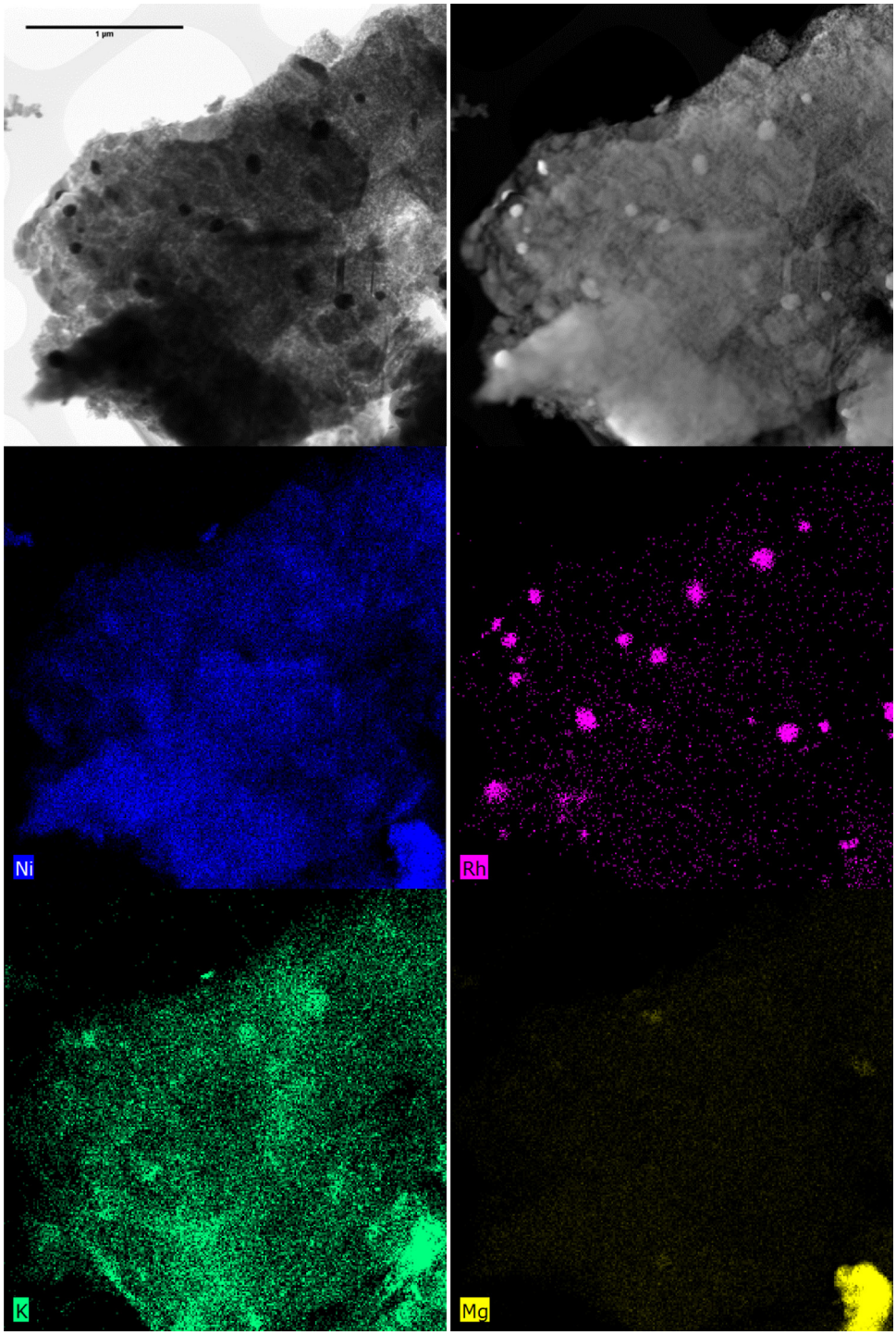

Fig. 14. Bright field, high angle annular dark field (HAADF) TEM images and TEM-EDS elemental distribution for Ni, noble metal promoter Rh, K and Mg on spent Rh-Ni catalyst from pinewood RFV. Reaction conditions: Pinewood flow rate = 15 g/h, Temperature = 750 °C, C/O = 0.68, C/S = 1.17 and Runtime = 260 min.

may explain the slight agglomeration. Both fresh and used catalysts exhibit diffraction peaks at 2θ of 45.86° and 67.03°, which is a clear evidence of the existence of γ–alumina phase (JCPDS 10-0425, 29-0063 and 50-0741). However, new peaks appeared in the used catalysts at 2θ of 31.80° and 60.11° corresponding to δ–alumina (JCPDS 16-0394 and 46-1131). The freshly calcined catalysts do not exhibit δ–alumina peaks, suggesting that alumina partial phase transformation occurred during gasification process. As pointed out in our previous publication, alumina phase transformation is primarily caused by steam rich hydrothermal conditions used in the experiments [6].

Diffraction peak corresponding to NiO (2 0 0) (JCPDS 71-1179) at 2θ of 43.28° can be seen in Fig. 10 for the spent Re-Ni and Rh-Ni catalysts, but not for Ru-Ni catalyst. This suggests that nickel nanoparticles are partially re-oxidized into NiO, which is consistent with the observation of gradual shift in activity towards CH_4 and C_2 compounds during RFV experiments. Unlike Re-Ni and Rh-Ni catalysts, XRD pattern of the fresh and spent Ru-Ni catalyst showed a much weaker peak at 2θ of 43.28°, implies the low presence of

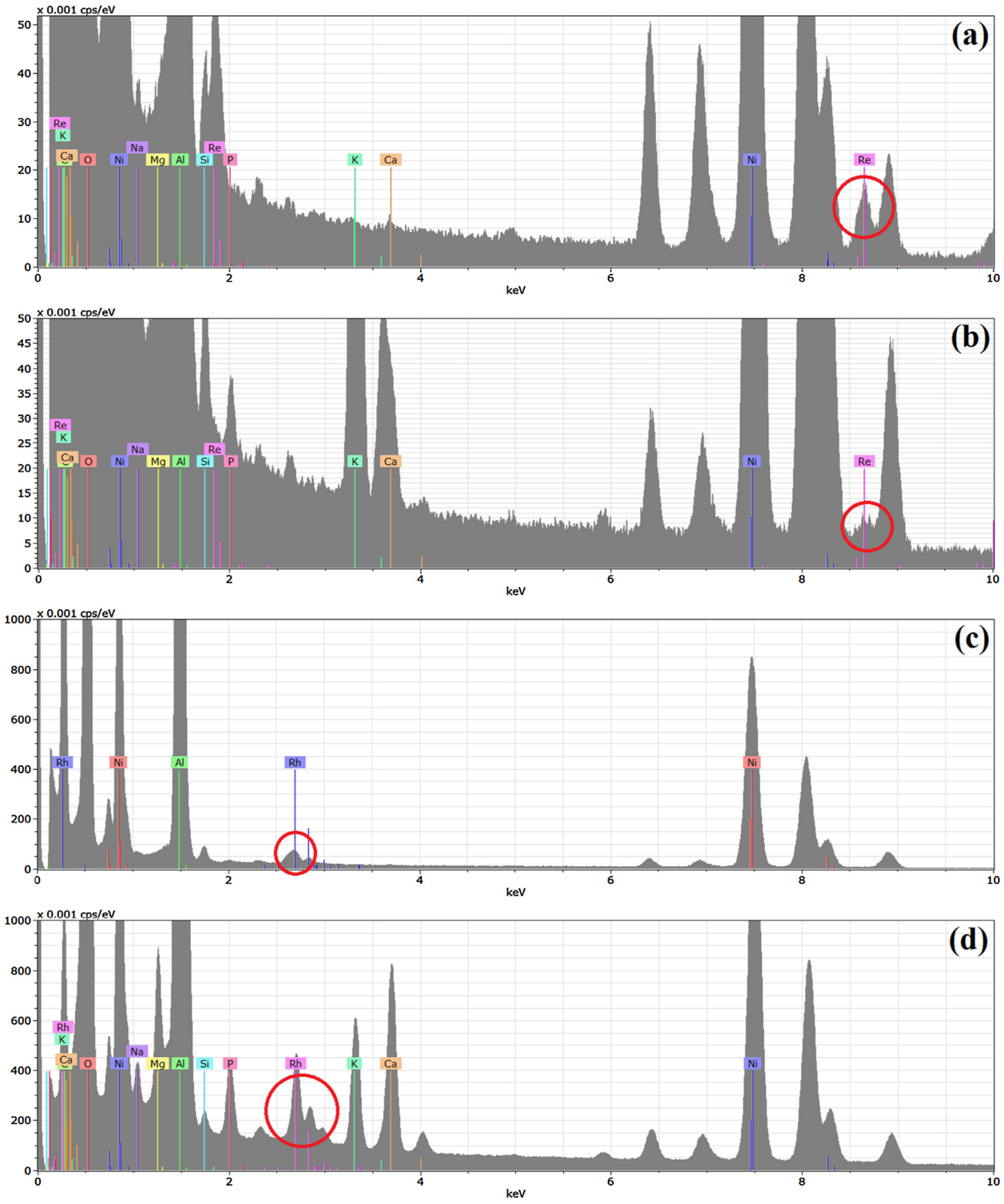

Fig. 15. TEM-EDS spectra of: (a) freshly reduced Re-Ni catalyst (b) Spent Re-Ni catalyst from pinewood RFV (Temp = 750 °C, C/O = 0.68, C/S = 1.17, TOS = 255 min) (c) freshly reduced Rh-Ni catalyst (d) Spent Rh-Ni catalyst from pinewood RFV (Temp = 750 °C, C/O = 0.68, C/S = 1.17, TOS = 260 min).

NiO on the catalyst. Two theories have been postulated based on this observation. First, the addition of Ru may help to promote the formation of Ru-Ni alloy and resulted in reduction of active Ni substrate. Second, the presence of Ru in bimetallic Ni-Ru systems does not prevent the solid-state diffusion of Ni^{2+} ions into the γ-$A1_2O_3$ lattice, as suggested by Rynkowski et al. [55]. Both theories are plausible and may help to explain the poor performance of Ru-Ni catalyst in RFV observed in this study. However, further examinations using X-Ray absorption study (EXAFS) are needed to verify these hypotheses.

EDS elemental mapping was carried out in scanning transmission electron microscopy (STEM) mode to study the distribution of metal nanoparticles on the freshly reduced catalysts and the spent catalysts, and to study the distribution of AAEM species on the spent catalysts to understand their interaction. Figs. 11 and 12 illustrate freshly reduced promoted nickel catalysts, which clearly

show finely distributed metal nanoparticles throughout the entire alumina support.

These figures confirm that the wet-impregnation technique used in this study was appropriate. EDS spectra of the freshly reduced Re-Ni and Rh-Ni catalysts are showed in Fig. 15(a) and (c), respectively. From the images, it can said that the Ni and noble metal are co-located in the nanoparticles, possibly as solid solutions (alloys), however, Extended X-ray Absorption Fine Structure (EXAFS) study using a synchrotron source is required to confirm this.

Figs. 13 and 14 show the mapping of various metals on the spent catalysts. These figures show that the potassium is finely distributed over catalyst surface but magnesium is phase segregated. This suggests that nickel nanoparticles may have strong interaction with K species during the RFV reaction. As a group 1A monovalent alkali metal, K is known to be highly reactive and electropositive [56]. It is particularly effective in promoting cellulose depolymerisation and steam gasification through interaction between carbon (solid) and steam (liquid) during gasification [57,58]. However, the high reactivity also poses another problem to the promoted nickel catalyst. Several reports have pointed out that K can react with Ni and causes deactivation in nickel catalyst by faceting the active Ni crystal planes to less active (1 1 1) plane [59–63]. In contrast, Mg was phase separated with nickel nanoparticles, which suggests that there was minimal interaction between these two species. Mg is less reactive in gasification compared to K, partly due to its bivalent property and partly resulted from the chemical status in the feedstock [9,64]. Since Mg is one of the nutrients needed for plant growth, Mg tends to react with organic counter ions and form complexes which are bound inside the cell wall and organelles, whereas majority of K remains in ionic form [64]. Because of this "caging effect", it is much harder for the Mg to "break free" from the feedstock which explains its lower catalytic activity in gasification compared to K.

From Fig. 13, it can be seen that the amount of Re detected on the spent Re-Ni catalyst was qualitatively lower than fresh Re-Ni catalyst, which is also illustrated in the EDS spectra (Fig. 15(b)). Re loss may be observed during high temperature reaction in the presence of excess oxygen due to the conversion of Re° into volatile Re heptoxide (Re_2O_7) [65]. This observation may also explain the gradual shift in product selectivity from CO to CH_4 observed during the RFV experiments. From Fig. 14, it can be seen that after the RFV reaction, the Rh nanoparticles were agglomerated on the spent Rh-Ni catalyst, whereas the fresh catalysts had well dispersed Rh nanoparticles. The Rh nanoparticle grew from <10 nm (fresh) to ~150 nm clusters after approximately 260 min of run. Reductive agglomeration of Rh^+ nanoparticles is induced by CO thermal desorption, which has been observed during steam reforming and hydrogenation reactions [66–70]. The increase in Rh nanoparticles size may reduce Rh-Ni catalytic activity, leading to char formation.

In summary, the extent of alumina phase transformation and carbon fouling of the promoted nickel catalysts were noticeably lower after RFV of pinewood and eucalyptus sawdust in comparison to RFV of cellulose. The deactivation of the catalyst mainly resulted from the partial oxidation of the nickel nanoparticles, sintering of Rh nanoparticles or partial loss of Re due to oxidation into volatile Re_2O_7 and partial loss of the surface area due to alumina phase transformation.

4. Conclusions

The gasification efficiency of promoted nickel catalyst in RFV of pinewood sawdust was in the following order: Re-Ni > Rh-Ni > Ru-Ni. Char free gasification was achieved with Re-Ni catalyst only at all the C/O ratios and C/S ratios in the RFV of pinewood and eucalyptus sawdust. Negligible quantity of carbon was detected in the condensate (tar + water) with all the catalysts tested in this part of the research. Higher catalytic activity was attributed to high metal dispersion of the active metals on the catalyst and high activity in promoting partial oxidation and reforming reactions.

Gasification efficiency of high ash content feedstock was found to be significantly higher than that of cellulose. This can be attributed to the effects of higher amorphous structure of lignocellulosic biomass compared to microcrystalline cellulose, and the catalytic effects of alkali and alkaline earth metals (AAEM species) found in the lignocellulosic biomass ash. However, results from RFV of pinewood and eucalyptus sawdust showed that the oxygen rich conditions used in this study was not suitable for biomass containing significant ash, since the final product gas contained high CO_2 content with lower calorific value. This was especially true for Re-Ni catalysts since in the oxygen rich conditions, Re was partially lost due to volatilisation as Re_2O_7. Reactive flash volatilisation was also catalysed by AAEM species and was found to be dominated by oxidation under these reaction conditions. Therefore, further studies under lower oxygen feed rate must be carried out. The noble metal promoters had lower effect on product yields and gas composition compared to cellulose gasification.

The deactivation of the promoted nickel catalyst used in this study was found to be substantially lower than the RFV of cellulose. Based on the XRD and TEM-EDS results, the main deactivation causes were the re-oxidation of the nickel nanoparticles, loss of surface area of Rh (sintering) and Re (volatilisation) and partial loss of the support surface area due to the alumina phase transformation.

Acknowledgements

The authors are grateful for the financial support from the Rural Industries Research and Development Corporation (RIRDC) project grant PRJ-004758 and the Department of Chemical Engineering, Monash University. The authors also acknowledge use of the facilities and the assistance of Dr Timothy Williams at the Monash Centre for Electron Microscopy.

References

[1] P. Alvira, E. Tomás-Pejó, M. Ballesteros, M.J. Negro, Bioresour. Technol. 101 (2010) 4851–4861.
[2] A. Demirbaş, Energy Convers. Manag. 42 (2001) 1357–1378.
[3] L. Devi, K.J. Ptasinski, F.J.J.G. Janssen, Biomass Bioenergy 24 (2003) 125–140.
[4] M. Verma, S. Godbout, S.K. Brar, O. Solomatnikova, S.P. Lemay, J.P. Larouche, Int. J. Chem. Eng. 2012 (2012) 18, http://dx.doi.org/10.1155/2012/542426, Article ID 542426.
[5] F.L. Chan, A. Tanksale, Renew. Sustain. Energy Rev. 38 (2014) 428–438.
[6] F.L. Chan, A. Tanksale, ChemCatChem 6 (2014) 2727–2739.
[7] R. Wooley, M. Ruth, D. Glassner, J. Sheehan, Biotechnol. Progr. 15 (1999) 794–803.
[8] B. Bals, C. Wedding, V. Balan, E. Sendich, B. Dale, Bioresour. Technol. 102 (2011) 1277–1283.
[9] M. Kajita, T. Kimura, K. Norinaga, C.-Z. Li, J.-i. Hayashi, Energy Fuels 24 (2010) 108–116.
[10] K. Yip, F. Tian, J.-i. Hayashi, H. Wu, Energy Fuels 24 (2010) 173–181.
[11] K. Mitsuoka, S. Hayashi, H. Amano, K. Kayahara, E. Sasaoaka, M.A. Uddin, Fuel Process. Technol. 92 (2011) 26–31.
[12] G. Yildiz, F. Ronsse, R. Venderbosch, R.v. Duren, S.R.A. Kersten, W. Prins, Appl. Catal. B: Environ. 168–169 (2015) 203–211.
[13] A. Nzihou, B. Stanmore, P. Sharrock, Energy 58 (2013) 305–317.
[14] F.L. Chan, K. Umeki, A. Tanksale, ChemCatChem 7 (2015) 1329–1337.
[15] R.F.H. Dekker, Biocatal. Biotransform. 1 (1987) 63–75.
[16] K.K.Y. Wong, K.F. Deverell, K.L. Mackie, T.A. Clark, L.A. Donaldson, Biotechnol. Bioeng. 31 (1988) 447–456.
[17] A. Ferraz, J. Baeza, J. Rodriguez, J. Freer, Bioresour. Technol. 74 (2000) 201–212.
[18] H. Kawamoto, H. Morisaki, S. Saka, J. Anal. Appl. Pyrolysis 85 (2009) 247–251.
[19] F. Ronsse, X. Bai, W. Prins, R.C. Brown, Environ. Prog. Sustain. Energy 31 (2012) 256–260.
[20] D.K. Shen, S. Gu, Bioresour. Technol. 100 (2009) 6496–6504.
[21] P. Giudicianni, G. Cardone, R. Ragucci, J. Anal. Appl. Pyrolysis 100 (2013) 213–222.
[22] T. Hosoya, H. Kawamoto, S. Saka, J. Anal. Appl. Pyrolysis 80 (2007) 118–125.

[23] M. Asmadi, H. Kawamoto, S. Saka, Holzforschung 66 (2012) 323–330.
[24] D.S. Scott, L. Paterson, J. Piskorz, D. Radlein, J. Anal. Appl. Pyrolysis 57 (2001) 169–176.
[25] C. Di Blasi, A. Galgano, C. Branca, Ind. Eng. Chem. Res. 48 (2009) 3359–3369.
[26] H. Wu, K. Yip, F. Tian, Z. Xie, C.Z. Li, Ind. Eng. Chem. Res. 48 (2009) 10431–10438.
[27] E.A. Ison, J.E. Cessarich, N.E. Travia, P.E. Fanwick, M.M. Abu-Omar, J. Am. Chem. Soc. 129 (2007) 1167–1178.
[28] R. Pérez-Hernández, A. Gutiérrez-Martínez, C.E. Gutiérrez-Wing, Int. J. Hydrog. Energy 32 (2007) 2888–2894.
[29] A. Godula-Jopek, W. Jehle, J. Wellnitz, Hydrogen Storage Technologies: New Materials, Transport, and Infrastructure, Wiley, 2012.
[30] S. Eriksson, S. Rojas, M. Boutonnet, J.L.G. Fierro, Appl. Catal. A: Gen. 326 (2007) 8–16.
[31] R. Horn, K.A. Williams, N.J. Degenstein, A. Bitsch-Larsen, D. Dalle Nogare, S.A. Tupy, L.D. Schmidt, J. Catal. 249 (2007) 380–393.
[32] E. Kantarelis, W. Yang, W. Blasiak, Energy Fuels 27 (2013) 4748–4759.
[33] R.P. KibbleWhite, M.J.C. Riddell, C.J.A. Shelbourne, N. Z. J. For. Sci. 30 (2000) 458–474.
[34] M. Brink, E.G. Achigan-Dako, Fibres, PROTA Foundation, 2012.
[35] G. Koch, Handbook of Pulp, Wiley-VCH Verlag GmbH, 2008, pp. 21–68.
[36] M.G. Grønli, G. Várhegyi, C. Di Blasi, Ind. Eng. Chem. Res. 41 (2002) 4201–4208.
[37] T.E. Timell, Wood Sci. Technol. 1 (1967) 45–70.
[38] P. Reyes, R.T. Mendonca, J. Rodriguez, P. Fardim, B. Vega, J. Chil. Chem. Soc. 58 (2013) 1614–1618.
[39] C. Stewart, D. Foster, Aust. J. Chem. 6 (1953) 431–438.
[40] C. Di Blasi, C. Branca, A. Santoro, E. Gonzalez Hernandez, Combust. Flame 124 (2001) 165–177.
[41] X. Li, E. Ximenes, Y. Kim, M. Slininger, R. Meilan, M. Ladisch, C. Chapple, Biotechnol. Biofuels 3 (2010) 1–7.
[42] J.J. Stewart, T. Akiyama, C. Chapple, J. Ralph, S.D. Mansfield, Plant Physiol. 150 (2009) 621–635.
[43] H. Kawamoto, M. Murayama, S. Saka, J. Wood Sci. 49 (2003) 469–473.
[44] Y.C. Lin, J. Cho, G.A. Tompsett, P.R. Westmoreland, G.W. Huber, J. Phys. Chem. C 113 (2009) 20097–20107.
[45] P.R. Patwardhan, J.A. Satrio, R.C. Brown, B.H. Shanks, Bioresour. Technol. 101 (2010) 4646–4655.
[46] A. Demirbas, Prog. Energy Combust. Sci. 31 (2005) 171–192.
[47] A. Aho, N. DeMartini, A. Pranovich, J. Krogell, N. Kumar, K. Eränen, B. Holmbom, T. Salmi, M. Hupa, D.Y. Murzin, Bioresour. Technol. 128 (2013) 22–29.
[48] Y. Sekiguchi, F. Shafizadeh, J. Appl. Polym. Sci. 29 (1984) 1267–1286.
[49] G. Nahar, V. Dupont, M.V. Twigg, E. Dvininov, Appl. Catal. B: Environ. 168–169 (2015) 228–242.
[50] P. Van Beurden, Energy Research Centre of the Netherlands (ECN), Technical Report I-04-003 (2004).
[51] L.a. Garcia, R. French, S. Czernik, E. Chornet, Appl. Catal. A: Gen. 201 (2000) 225–239.
[52] A. Le Valant, N. Bion, F. Can, D. Duprez, F. Epron, Appl. Catal. B: Environ. 97 (2010) 72–81.
[53] F. Abild-Pedersen, O. Lytken, J. Engbæk, G. Nielsen, I. Chorkendorff, J.K. Nørskov, Surf. Sci. 590 (2005) 127–137.
[54] K. Engelen, Y. Zhang, D.J. Draelants, G.V. Baron, Chem. Eng. Sci. 58 (2003) 665–670.
[55] J.M. Rynkowski, T. Paryjczak, M. Lenik, Appl. Catal. A: Gen. 126 (1995) 257–271.
[56] Z. Abu El-Rub, E.A. Bramer, G. Brem, Ind. Eng. Chem. Res. 43 (2004) 6911–6919.
[57] N. Padban, PFB Air Gasification of Biomass, Investigation of Product Formation and Problematic Issues Related to Ammonia, Tar and Alkali, Lund University, Ingemar Odenbrand, Department of Chemical Engineering II, Lund University, 2000.
[58] A.A. Lizzio, L.R. Radovic, Ind. Eng. Chem. Res. 30 (1991) 1735–1744.
[59] R.J. Berger, E.B.M. Doesburg, J.G. van Ommen, J.R.H. Ross, Appl. Catal. A: Gen. 143 (1996) 343–365.
[60] K. Sugiura, M. Yamauchi, K. Tanimoto, Y. Yoshitani, J. Power Sources 145 (2005) 199–205.
[61] J.R. Rostrup-Nielsen, L.J. Christiansen, Appl. Catal. A: Gen. 126 (1995) 381–390.
[62] S. Cavallaro, V. Chiodo, S. Freni, N. Mondello, F. Frusteri, Appl. Catal. A: Gen. 249 (2003) 119–128.
[63] F. Frusteri, S. Freni, V. Chiodo, L. Spadaro, O. Di Blasi, G. Bonura, S. Cavallaro, Appl. Catal. A: Gen. 270 (2004) 1–7.
[64] D.M. Keown, J.-i. Hayashi, C.-Z. Li, Fuel 87 (2008) 1187–1194.
[65] K. Bouchmella, M. Stoyanova, U. Rodemerck, D.P. Debecker, P. Hubert Mutin, Catal. Commun. 58 (2015) 183–186.
[66] R.B. Duarte, M. Nachtegaal, J.M.C. Bueno, J.A. van Bokhoven, J. Catal. 296 (2012) 86–98.
[67] G.S. Fonseca, A.P. Umpierre, P.F.P. Fichtner, S.R. Teixeira, J. Dupont, Chem.—A Eur. J. 9 (2003) 3263–3269.
[68] F. Solymosi, T. Bánsági, É. Novák, J. Catal. 112 (1988) 183–193.
[69] F. Solymosi, H. Knozinger, J. Chem. Soc. Faraday Trans. 86 (1990) 389–395.
[70] S. Trautmann, M. Baerns, J. Catal. 150 (1994) 335–344.